

Supporting Information

Tailoring Electronic Structure of O3-Type Layered Oxide Cathode to Achieve Long-Cycle and High-Rate Sodium-Ion Batteries

Yuheng Gao¹, Guohua Zhang^{2,*}, Yongsheng Ji², Zhiqi Yang², Yuxin Fan², Xuemin Shi², Yunhui Huang^{1,*}

¹State Key Laboratory of Material Processing and Die & Mould Technology, School of Materials Science and Engineering, Huazhong University of Science and Technology, Wuhan, Hubei 430074, China

²Institute of New Energy for Vehicles, Shanghai Key Laboratory for R&D and Application of Metallic Functional Materials, School of Materials Science and Engineering, Tongji University, Shanghai 201804, China

*Corresponding author.

E-mail addresses: huangyh@hust.edu.cn (Y. Huang), 2011580@tongji.edu.cn (G. Zhang)

Experimental section

Materials Synthesis

The $\text{Na}_{0.98}\text{Ni}_{0.22}\text{Fe}_{0.28}\text{Mn}_{0.5}\text{O}_2$ (NFM), $\text{Na}_{0.98}\text{Co}_{0.05}\text{Ni}_{0.22}\text{Fe}_{0.23}\text{Mn}_{0.5}\text{O}_2$ (CNFM), $\text{Na}_{0.98}\text{Li}_{0.03}\text{Ni}_{0.22}\text{Fe}_{0.25}\text{Mn}_{0.5}\text{O}_2$ (LNFM), and $\text{Na}_{0.98}\text{Li}_{0.03}\text{Co}_{0.05}\text{Ni}_{0.22}\text{Fe}_{0.2}\text{Mn}_{0.5}\text{O}_2$ (LCNFM) samples were synthesized by a simple solid-state method. The stoichiometric ratio of Na_2CO_3 (Aladdin, 99.8%), MnO_2 (Aladdin, 98%), Fe_2O_3 (Aladdin, 99.9%), NiO (Aladdin, 99%), Li_2CO_3 (Aladdin, 99%) and CoO (Aladdin, 99.5%) were thoroughly mixed by ball-milling at 500 rpm for 10 h, and then the mixtures were pressed into tablets. An additional 5% of Na_2CO_3 and 5% of Li_2CO_3 were added to account for potential losses during the preparation process. The tablets were sintered at 500 °C for 5 h, followed by 900 °C for 15 h with a ramping rate of 5 °C/min in an oxygen atmosphere and then naturally cooled to room temperature. Finally, the obtained target samples were transferred to an Ar-filled glovebox.

Materials characterizations

The structure of the samples was confirmed by an X-Ray Diffractometer (Bruker D8) with Cu $K\alpha$ radiation ($\lambda = 1.5406 \text{ \AA}$). Rietveld refinement was conducted to analyze the powder XRD patterns using FullProf software. Field-emission scanning electron microscopy (SEM, JSM-6390) assembled with energy dispersive spectroscopy (EDS) and high-resolution transmission electron microscope (HR-TEM, JEM 2100F, 200 kV) were used to investigate the morphologies and crystal structures of the materials. XPS measurements were performed on an Escalab 250Xi (Thermo Fisher Scientific) with an Al $K\alpha$ radiation (1486.6 eV).

Electrochemistry Measurements

The positive electrodes were prepared by smearing the slurries consist of 80 wt.% active material, 10 wt.% conductive agents (Super P), and 10 wt.% polyvinylidene fluoride (PVDF) binder with a suitable amount of N-methyl-2-pyrrolidone (NMP) solution onto an aluminum foil, and followed drying at 100 °C in the vacuum oven. The as-prepared electrodes were punched into disks of 12 mm in diameter with a mass loading of about 3.5 mg/cm². sodium metal and glass fiber (GF/B, Whatman) were used as the anode electrode and separator, respectively. 1.0 M NaClO_4 in propylene carbonate (PC), ethylene carbonate (EC) and dimethyl carbonate (DMC) solution (1:1:1 by volume)

with 5 vol% fluoroethylene carbonate (FEC) additive was used as the electrolyte. The half cells were assembled in Ar-filled glove box. The galvanostatic charge/discharge tests were conducted on both LAND (CT2001A, Wuhan Jinnuo Electronics Co., Ltd.) and Neware battery testing systems in the voltage range of 2.0–4.0 V vs. Na⁺/Na at 25 °C. The cyclic voltammetry measurements were performed on an electrochemical workstation with a scan rate of 0.1 mV/s. Galvanostatic intermittent titration technique (GITT) profiles were tested at 0.1 C for 30 min, then sit for 10 h on a Neware battery testing system. The Na⁺ diffusion coefficients (D_{Na^+}) could be calculated by the following equation:

$$D_{\text{Na}^+} = \frac{4}{\pi\tau} \left(\frac{m_B V_m}{M_B S} \right)^2 \left(\frac{\Delta E_s}{\Delta E_\tau} \right)^2$$

Where τ is the relaxation time of a single current pulse, m_B , V_m and M_B are the mass (g), molar volume ($\text{cm}^3 \text{mol}^{-1}$) and molar mass (g mol^{-1}) of the active substance in the electrode, respectively, S is the effective contact area between electrode and electrolyte, ΔE_s is the value change of the adjacent steady-state voltage, and ΔE_τ is the voltage change induced by a current pulse.

Theoretical computations

Density functional theory (DFT) calculations were carried out using the Vienna Ab initio Simulation Package (VASP) code.¹ The exchange-correlation interaction was modeled with the Perdew–Burke–Ernzerhof (PBE) functional under the generalized gradient approximation (GGA).² The projector augmented wave (PAW) pseudopotential was applied with a plane wave cutoff energy of 500 eV to expand the electronic wavefunctions.³ A 25 Å thick vacuum slab was used to minimize interlayer interactions. The Brillouin zone was sampled with a $5 \times 5 \times 1$ Γ -centered Monkhorst-Pack k-point mesh. All atomic positions were fully relaxed until the energy and residual force converged to 10^{-5} eV and 0.03 eV/Å, respectively. Long-range dispersion interactions were accounted for using the DFT-D method.⁴ The minimum energy pathway and corresponding activation barrier for the cyclization reaction were obtained using the climbing image nudged elastic band (CI-NEB) method.

The d-band center ϵ_d is a calculated value often used to characterize the catalytic properties of transition metals. It represents the distribution of d-electrons near the Fermi level, giving insight

into the interaction strength between the metal and reactants. The formula for calculating the d-band center ϵ_d given the density of states $D(E)$ of the d-states is:

$$\epsilon_d = \frac{\int_{-\infty}^{\infty} E \cdot D(E) dE}{\int_{-\infty}^{\infty} D(E) dE}$$

where:

E is the energy;

$D(E)$ is the density of d-states at energy E ;

The numerator $\int_{-\infty}^{\infty} E \cdot D(E) dE$ represents the weighted energy of the d-electrons;

The denominator $\int_{-\infty}^{\infty} D(E) dE$ is the total d-state density.

Table S1. ICP-OES data of NFM, CNFM, LNFM and LCNFM samples.

Samples	Na	Ni	Fe	Mn	Cu	Li
NFM	0.97(7)	0.21(9)	0.28(3)	0.50(2)	—	—
CNFM	0.97(8)	0.22(5)	0.23(4)	0.49(9)	0.04(9)	—
LNFM	0.98(2)	0.22(3)	0.25(2)	0.49(8)	—	0.03(2)
LCNFM	0.98(3)	0.21(8)	0.19(9)	0.50(3)	0.05(2)	0.03(1)

Table S2. Structural information of NFM, CNFM, LNFM and LCNFM obtained from Rietveld refinements.

NFM

Atom	Site	<i>x</i>	<i>y</i>	<i>z</i>	Occ.
O	6c	0	0	0.2348	1
Fe	3b	0	0	0.5	0.28
Mn	3b	0	0	0.5	0.50
Ni	3b	0	0	0.5	0.22
Na	3a	0	0	0	0.98

Space group $R\bar{3}m$. $a = b = 2.94360(5)$ Å, $c = 16.37418(4)$ Å, $V = 122.871$ Å³. $R_p = 2.28\%$, $R_{wp} = 3.11\%$, $R_{exp} = 2.18\%$, $\chi^2 = 2.03$.

CNFM

Atom	Site	<i>x</i>	<i>y</i>	<i>z</i>	Occ.
O	6c	0	0	0.2348	1
Fe	3b	0	0	0.5	0.23
Mn	3b	0	0	0.5	0.5
Ni	3b	0	0	0.5	0.22
Na	3a	0	0	0	0.98
Co	3b	0	0	0.5	0.05

Space group $R\bar{3}m$. $a = b = 2.93382(3)$ Å, $c = 16.36314(4)$ Å, $V = 120.973$ Å³. $R_p = 2.17\%$, $R_{wp} = 2.87\%$, $R_{exp} = 2.20\%$, $\chi^2 = 1.70$.

LNFM

Atom	Site	x	y	z	Occ.
O	6c	0	0	0.2348	1
Fe	3b	0	0	0.5	0.25
Mn	3b	0	0	0.5	0.5
Ni	3b	0	0	0.5	0.22
Na	3a	0	0	0	0.98
Li	3b	0	0	0.5	0.03

Space group $R\bar{3}m$. $a = b = 2.94671(7)$ Å, $c = 16.21312(9)$ Å, $V = 121.920$ Å³. $R_p = 2.26\%$, $R_{wp} = 2.96\%$, $R_{exp} = 2.29\%$, $\chi^2 = 1.67$.

LCNFM

Atom	Site	x	y	z	Occ.
O	6c	0	0	0.2348	1
Fe	3b	0	0	0.5	0.2
Mn	3b	0	0	0.5	0.5
Ni	3b	0	0	0.5	0.22
Na	3a	0	0	0	0.98
Li	3b	0	0	0.5	0.03
Co	3b	0	0	0.5	0.05

Space group $R\bar{3}m$. $a = b = 2.93562(5)$ Å, $c = 16.21706(8)$ Å, $V = 121.033$ Å³. $R_p = 2.19\%$, $R_{wp} = 2.91\%$, $R_{exp} = 2.16\%$, $\chi^2 = 1.80$.

Table S3. Comparisons of the lattice parameters among NFM, CNFM, LNFM and LCNFM samples.

Samples	$a = b$ (Å)	c (Å)	V (Å ³)
NFM	2.9436	16.3742	122.871
CNFM	2.9338	16.3631	121.973
LNFM	2.9467	16.2131	121.920
LCNFM	2.9356	16.2171	121.033

Table S4. The lengths of Mn–O bonds and distances of Na⁺ layers from Rietveld refinement results for as-prepared samples.

Samples	NFM	CNFM	LNFM	LCNFM
$d_{\text{Mn-O}}$ (Å)	2.0329	2.0278	2.0284	2.0232
$d_{\text{O-Na-O}}$ (Å)	3.2269	3.2246	3.1951	3.1959

Table S5. Comparison of the electrochemical performance of O3-type layered cathode materials for sodium ion batteries

Cathode materials	Voltage range	Initial capacity	Cycle retention ratio	Ref.
O3-Na _{1.0} Li _{0.1} Ni _{0.3} Fe _{0.1} Mn _{0.25} Ti _{0.25} O ₂	2.0–4.0 V	123 mAh g ⁻¹	88% after 200 cycles (1 C) 77% after 400 cycles (2 C)	5
O3-Na _{0.9} Ni _{0.2} Fe _{0.2} Co _{0.2} Mn _{0.2} Ti _{0.15} Cu _{0.05} O ₂	2.2–4.1 V	117.7 mAh g ⁻¹	70.7% after 1000 cycles (1 C) 79.4% after 2000 cycles (5 C)	6
O3-NaNi _{0.12} Cu _{0.12} Mg _{0.12} Fe _{0.15} Co _{0.15} Mn _{0.1} Ti _{0.1} Sn _{0.1} Sb _{0.04} O ₂	2.0–3.9 V	110 mAh g ⁻¹	79% after 200 cycles (1 C) 83% after 500 cycles (3 C)	7
O3-Na _{0.9} Li _{0.1} Ni _{0.4} Fe _{0.2} Mn _{0.4} Ti _{0.04} Mn _{0.04} Mg _{0.02} O _{1.9} F _{0.1}	2.0–4.0 V	109 mAh g ⁻¹	90% after 200 cycles (0.5 C)	8
O3-Na _{0.83} Li _{0.1} Ni _{0.25} Co _{0.2} Mn _{0.15} Ti _{0.15} Sn _{0.15} O _{2-δ}	2.0–4.2 V	109.4 mAh g ⁻¹	87.2% after 200 cycles (2 C)	9
O3-NaNi _{0.1} Mn _{0.15} Co _{0.2} Cu _{0.1} Fe _{0.1} Li _{0.1} Ti _{0.15} Sn _{0.1} O ₂	2.0–4.1 V	115 mAh g ⁻¹	82.7% after 1000 cycles (160 mA g ⁻¹)	10
O3-Na _{0.9} Ni _{0.25} Mn _{0.4} Fe _{0.2} Mg _{0.1} Ti _{0.05} O ₂	2.0–4.0 V	100.8 mAh g ⁻¹	85.7% after 300 cycles (1 C)	11
O3-NaFe _{0.2} Co _{0.2} Ni _{0.2} Ti _{0.2} Sn _{0.1} Li _{0.1} O ₂	2.0–4.1 V	112.7 mAh g ⁻¹	67% after 200 cycles (0.5 C)	12
O3-Na _{0.93} Li _{0.12} Ni _{0.25} Fe _{0.15} Mn _{0.48} O ₂	2.5–4.2 V	130.1 mAh g ⁻¹	82.8% after 200 cycles (1600 mA g ⁻¹)	13
O3-NaNi _{0.25} Mg _{0.05} Cu _{0.1} Fe _{0.2} Mn _{0.2} Ti _{0.1} Sn _{0.1} O ₂	2.0–4.0 V	130.8 mAh g ⁻¹	75% after 500 cycles (1 C)	14
spinel@O3-type Na _{0.9} Mn _{0.5} Ni _{0.5} Cu _{0.1} O _{2+x}	2.0–4.0 V	113 mAh g ⁻¹	82.5% after 280 cycles (1 C) 70% after 1000 cycles (5 C)	15
O3-Na _{0.98} Li _{0.03} Co _{0.05} Ni _{0.22} Fe _{0.2} Mn _{0.5} O ₂	2.0–4.0 V	112.1 mAh g ⁻¹	82.6% after 500 cycles (1 C) 87.2% after 1000 cycles (5 C)	This work

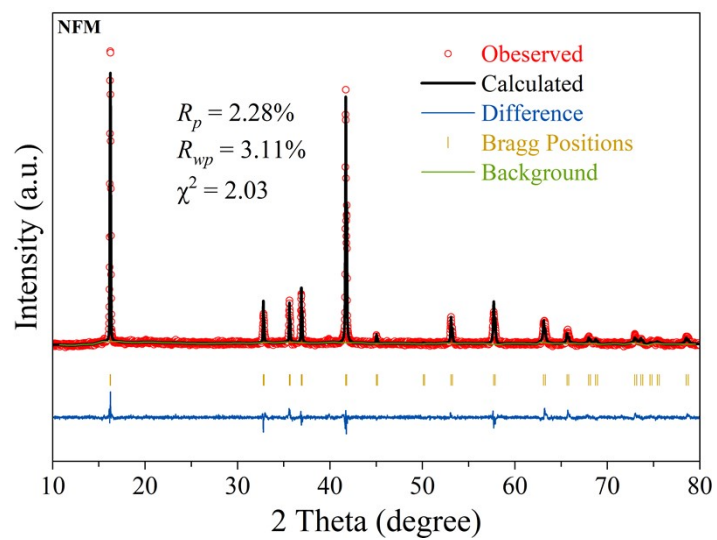


Fig. S1. Rietveld refinements of the XRD patterns of NFM

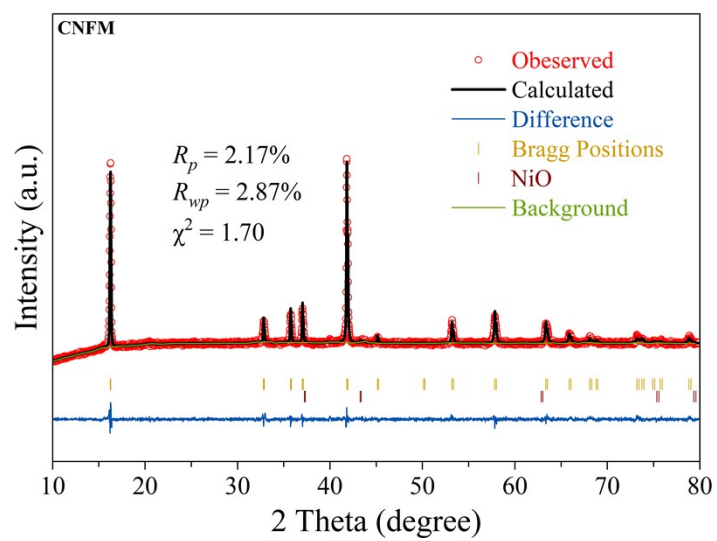


Fig. S2. Rietveld refinements of the XRD patterns of CNFM

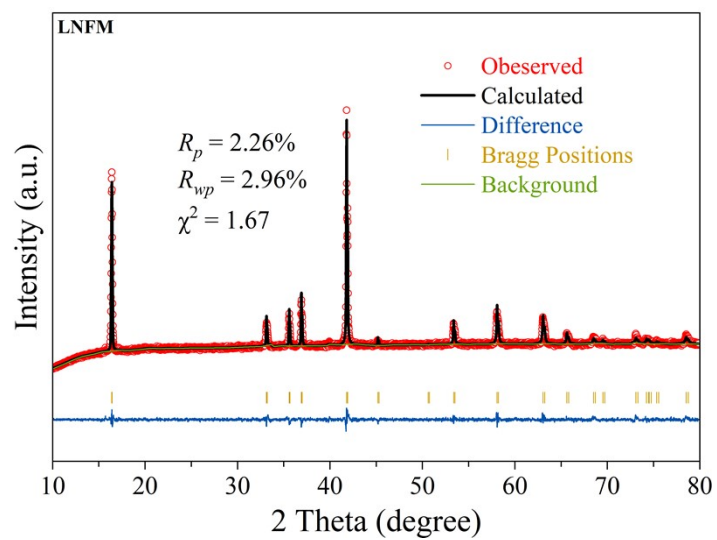


Fig. S3. Rietveld refinements of the XRD patterns of LNFM

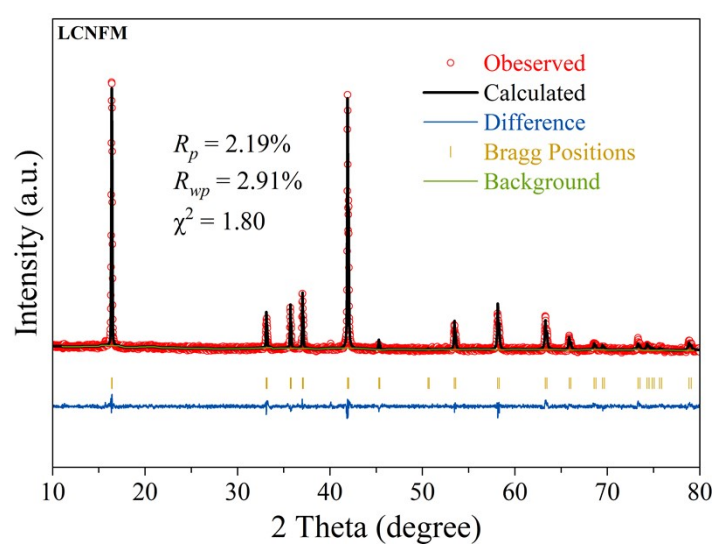


Fig. S4. Rietveld refinements of the XRD patterns of LCNFM.

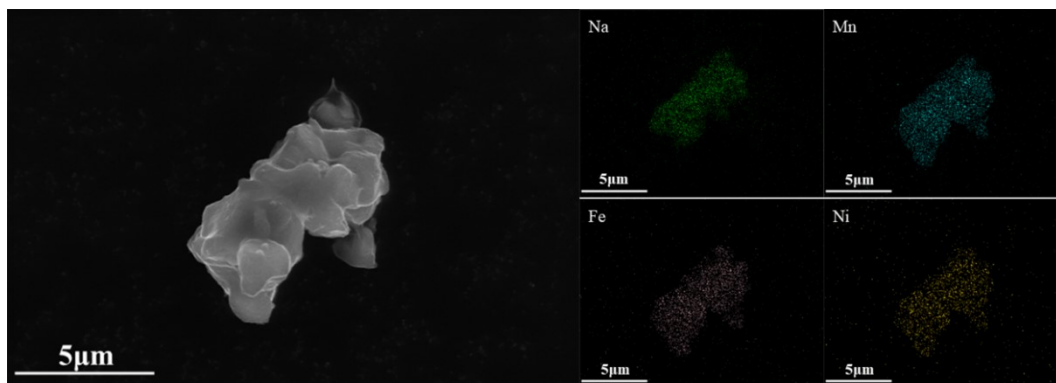


Fig. S5. SEM-EDS mapping images of NFM.

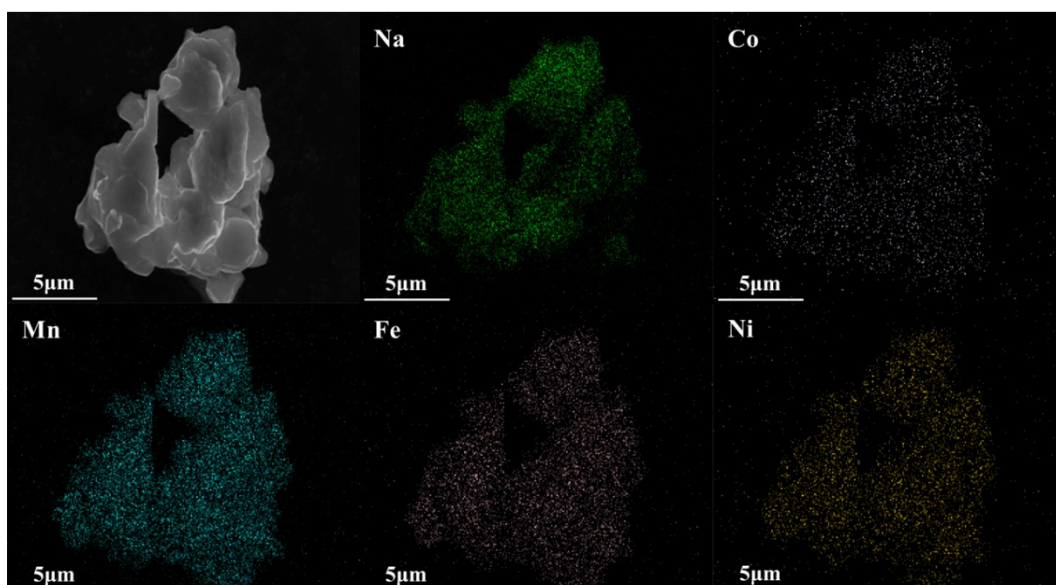


Fig. S6. SEM-EDS mapping images of LCNFM.

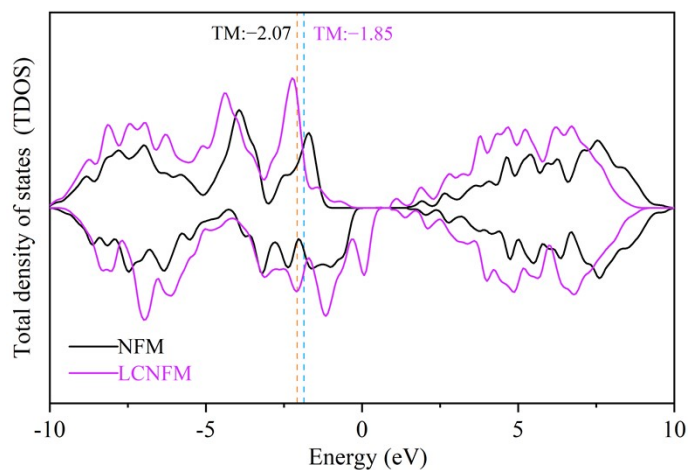


Fig. S7. Total density of states (TDOS) of NFM and LCNFM. The total d-band center of transition metals, including Ni, Fe, and Mn, shifts from -2.07 eV to -1.85 eV.

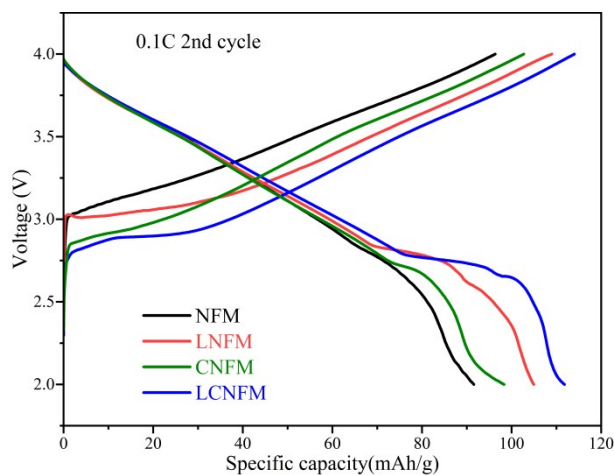


Fig. S8. Comparison of charge-discharge curves of the second cycle at 0.1 C rate in a voltage range of 2.0–4.0 V vs. Na^+/Na at 25°C between NFM, CNFM, LNFM and LCNFM.

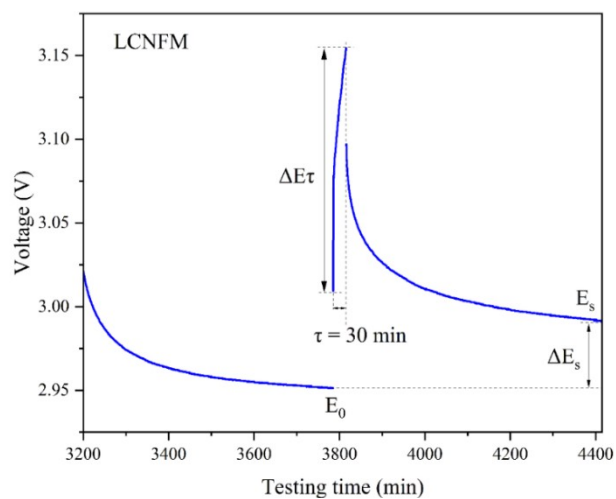


Fig. S9. Voltage vs time profiles for a single titration of a GITT experiment of LCNFM.

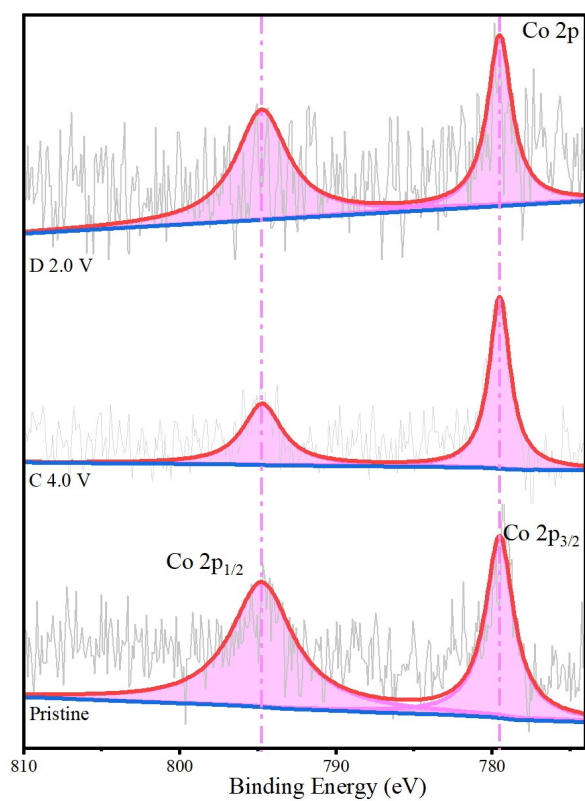


Fig. S10. XPS spectra of LCNFM for Co 2p.

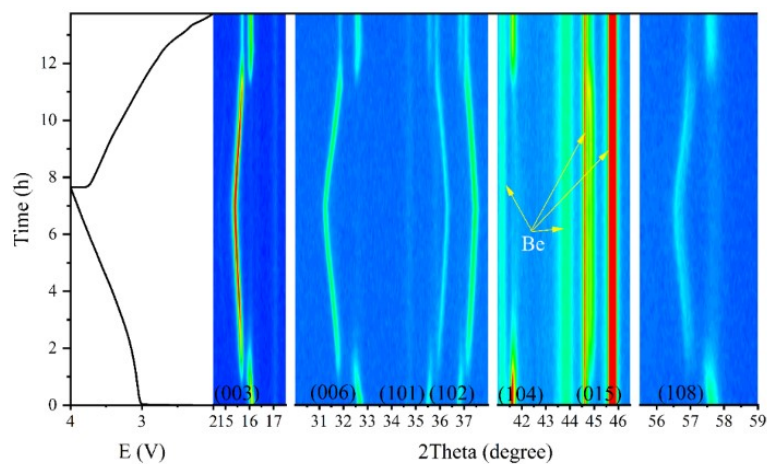


Fig. S11. Contour plots of *in-situ* XRD for the NFM electrode during the first charge/discharge process at 0.1 C in the voltage range of 2.0–4.0 V.

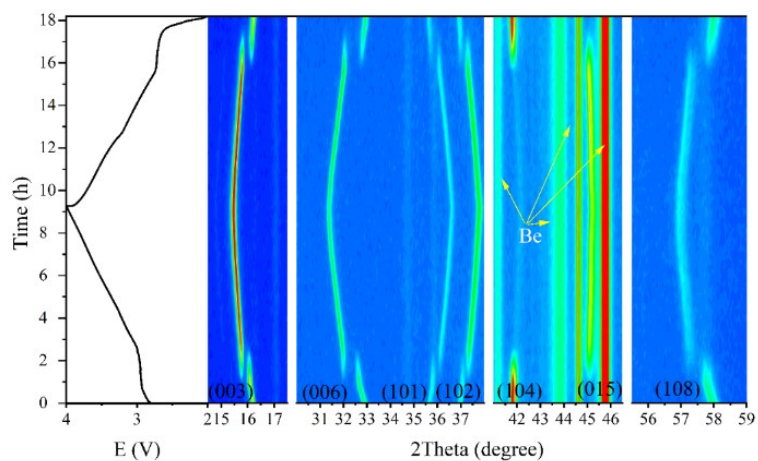


Fig. S12. Contour plots of *in-situ* XRD for the LCNFM electrode during the first charge/discharge process at 0.1 C in the voltage range of 2.0–4.0 V.

References:

1. G. Kresse and J. Furthmüller, *Comput. Mater. Sci.*, 1996, **6** 15-50.
2. J. P. Perdew, K. Burke and M. Ernzerhof, *Phys. Rev. Lett.*, 1996, **77**, 3865-3868.
3. P. E. Blöchl, *Phys. Rev. B*, 1994, **50**, 17953-17979.
4. S. Grimme, *J. Comput. Chem.*, 2006, **27**, 1787-1799.
5. A. Ghosh, R. Hegde and P. Senguttuvan, *J. Mater. Chem. A*, 2024, **12**, 14583-14594.
6. X. Z. Wang, Y. Zuo, Y. Qin, X. Zhu, S. W. Xu, Y. J. Guo, T. Yan, L. Zhang, Z. Gao, L. Yu, M. Liu, Y. X. Yin, Y. Cheng, P. F. Wang and Y. G. Guo, *Adv. Mater.*, 2024, e2312300.
7. C. Zhao, F. Ding, Y. Lu, L. Chen and Y. S. Hu, *Angew. Chem. Int. Ed.*, 2020, **59**, 264-269.
8. A. Joshi, S. Chakrabarty, S. H. Akella, A. Saha, A. Mukherjee, B. Schmerling, M. Ejgenberg, R. Sharma and M. Noked, *Adv. Mater.*, 2023, **35**, 2304440.
9. H. Wang, X. Gao, S. Zhang, Y. Mei, L. Ni, J. Gao, H. Liu, N. Hong, B. Zhang, F. Zhu, W. Deng, G. Zou, H. Hou, X. Y. Cao, H. Chen and X. Ji, *ACS Nano*, 2023, **17**, 12530-12543.
10. X. Y. Du, Y. Meng, H. Y. Yuan and D. Xiao, *Energy Storage Mater.*, 2023, **56**, 132-140.
11. L. Feng, J. Guo, C. Sun, X. Xiao, L. Feng, Y. Hao, G. Sun, Z. Tian, T. Li, Y. Li and Y. Jiang, *Small*, 2024, e2403084.
12. K. H. Tian, H. He, X. Li, D. Wang, Z. Y. Wang, R. G. Zheng, H. Y. Sun, Y. G. Liu and Q. C. Wang, *J. Mater. Chem. A*, 2022, **10**, 14943-14953.
13. X. G. Yuan, Y. J. Guo, L. Gan, X. A. Yang, W. H. He, X. S. Zhang, Y. X. Yin, S. Xin, H. R. Yao, Z. Huang and Y. G. Guo, *Adv. Funct. Mater.*, 2022, **32**.
14. F. Ding, C. Zhao, D. Xiao, X. Rong, H. Wang, Y. Li, Y. Yang, Y. Lu and Y. S. Hu, *J. Am. Chem. Soc.*, 2022, **144**, 8286-8295.
15. M. Li, H. Zhuo, M. Song, Y. Gu, X. Yang, C. Li, Z. Liao, Y. Ye, C. Zhao, Y. Jiang, J. Liang, D. Wang, K. Wang, D. Geng and B. Xiao, *Nano Energy*, 2024, **123**, 109375.